THE ASTRONOMICAL JOURNAL VOLUME 113, NUMBER 6 JUNE 1997

STELLAR POPULATIONS IN EDGE-ON GALAXIES FROM DEEP CCD SURFACE PHOTOMETRY. II. ONE-DIMENSIONAL FITS OF NGC 891

HEATHER L. MORRISON
Department of Astronomy and Department of Physics, Case Western Reserve University, Cleveland, Ohio 44106
Electronic mail: heather@vegemite.cwru.edu

ERIC D. MILLER[1]
Department of Physics, Oberlin College, Oberlin, Ohio 44074
Electronic mail: emiller@astro.lsa.umich.edu

PAUL HARDING
Steward Observatory, University of Arizona, Tucson, Arizona 85726
Electronic mail: harding@as.arizona.edu

DANIEL R. STINEBRING
Department of Physics, Oberlin College, Oberlin, Ohio 44074
Electronic mail: dan@physics.oberlin.edu

TODD A. BOROSON
US Gemini Program, National Optical Astronomy Observatories,[2] Tucson, Arizona 85726
Electronic mail: tyb@noao.edu

Received 1997 February 26; revised 1997 March 14

ABSTRACT

We present deep R-band CCD surface photometry of the nearby edge-on spiral NGC 891, which bears many similarities to the Milky Way. Our data confirm van der Kruit & Searle's (1981, A&A, 110, 61) finding that NGC 891 has a thick disk. We use one-dimensional fits of exponential disk models to averaged vertical profiles to show that this popular technique has a major drawback: it does not produce unique solutions when two or more stellar components are present, and no component dominates in the regions studied. For this galaxy, adequate fits are possible for thin disk scale heights ranging from 400–650 pc and thick disk scale heights from 1.5–2.5 kpc. Our next paper will use full two-dimensional modeling of the image to improve the fits. Although NGC 891 and the Milky Way have similar rotation curves and presumably similar total masses, and their disks have similar radial extent, NGC 891's disk and thick disk are both significantly more extended in the vertical direction. We suggest that the more extended thin disk may be caused by more efficient heating by NGC 891's more massive and thicker molecular cloud layer. The large thick disk scale height is harder to explain in the context of recent n-body simulations of thick disk formation via minor mergers, and shows the need for a more extensive exploration of parameter space in these models. © *1997 American Astronomical Society.* [S0004-6256(97)03006-9]

1. INTRODUCTION

Compared to the lifetime of a typical galaxy, the scant century of human observation of other galaxies is a brief span of time. Thus opportunities to watch galaxies forming directly are almost non-existent, and astronomers need to take one of two possible paths to study galaxy formation and evolution—study galaxies at very high redshift so we can observe them in the making; or depend on the "fossil record" of kinematics, position and metallicity of the older stars in a galaxy to tell us something about the conditions under which the galaxy formed. The exciting recent results on high-redshift galaxies and QSO absorption line systems (Steidel *et al.* 1996; Lanzetta *et al.* 1995; Morris *et al.* 1993) make it even more important to understand as much as we can of the history of nearby galaxies, so we do not misinterpret the necessarily more scanty high-redshift observations.

The study of thick disks is of particular interest for tracing early stages of disk evolution—in the Milky Way it has been established that the stars in its thick disk are the oldest and most metal-deficient disk stars (Carney *et al.* 1989; Edvardsson *et al.* 1993). Thus their properties might be expected to tell us much about the early stages of disk formation. One popular theory for thick disk formation (Quinn & Goodman 1986) suggests that a thick disk is formed when an existing

[1]Current address: Department of Astronomy, University of Michigan, Ann Arbor, MI 48109.
[2]The National Optical Astronomy Observatories are operated by the Association of Universities for Research in Astronomy, Inc. (AURA) under cooperative agreement with the National Science Foundation.

 0004-6256/97/113(6)/2061/14/$10.00

disk galaxy suffers a minor merger with a smaller satellite which heats the existing thin disk.

The existence of thick disks in spiral and S0 galaxies has been established for some time (Tsikoudi 1977; Burstein 1979; van der Kruit & Searle 1981a,1981b; Gilmore & Reid 1983). However, the faintness of this stellar component compared to both the more populous thin disk and to the night sky has made it hard to study in detail. Photographic surface photometry (employed by Tsikoudi, Burstein and van der Kruit and Searle) is not sufficiently precise for this purpose: deep CCD surface photometry is needed.

Morrison *et al.* (1994, hereafter MBH) have shown that it is possible to reach extremely faint using a large-format CCD mounted on a wide-field telescope. They reached to $R=27$ mag/sq. arcsec, 6 mag below sky. We have now made further improvements on these techniques, which have allowed us to study the edge-on galaxy NGC 891 despite the very large number of foreground stars obscuring the galaxy. A detailed discussion of the problems which need to be addressed in order to do good CCD surface photometry, and the solutions we have developed, can be found in Appendix A.

NGC 891 is a nearby edge-on galaxy of Hubble type Sb (see Fig. 1) (Plate 39). It bears a strong resemblance to our Galaxy in many respects (van der Kruit 1984; Scoville *et al.* 1993) and has a flat rotation curve with maximum at 225 km/s (Garcia-Burillo *et al.* 1992). Its disk subtends 10 arcminutes on the sky, and the galaxy is at a distance of 10 Mpc (Ciardullo *et al.* 1991). It is unusual in having bright diffuse Hα emission which stretches to 4.5 kpc above the plane of the disk (Rand & Kulkarni 1990).

NGC 891 was observed by van der Kruit & Searle (1981b, hereafter vdKS) using deep photographic surface photometry. They estimated photometric parameters of its thin disk, and also detected its thick disk. Their data were later re-analyzed by Bahcall & Kylafis (1985) and Shaw & Gilmore (1989) who made estimates of thick disk parameters.

The technique of one-dimensional fits to surface brightness profiles of the galaxy is a traditional one (e.g., Burstein 1979; Boroson 1981; van der Kruit & Searle 1981a) that has the advantage that it is easy to evaluate goodness of fit by inspecting the plots. It has been superseded by full two-dimensional fits (Bahcall & Kylafis 1985, Shaw & Gilmore 1989, MBH) but, perhaps because of the computational difficulty of implementing these algorithms, many workers still use the earlier method (e.g., Kent *et al.* 1991; de Grijs & van der Kruit 1996; Chen *et al.* 1997). We will show that one-dimensional fits to averaged vertical profiles are inadequate in the case where several stellar components overlap spatially.

Below we present our deep surface photometry of NGC 891 and our preliminary analysis of the data using one-dimensional surface brightness profiles, and show that our results confirm and extend previous work on this galaxy. The galaxy does indeed have a thick disk (clearly visible in the outer, faint regions of the galaxy in Fig. 1). We also discuss our findings in the context of the stellar populations of the Milky Way, and show that although in many ways the two galaxies are very similar, they do differ in several important respects.

2. OBSERVATIONS AND DATA REDUCTION

The data for this project were obtained on 4 nights in 1994 October/November using the Burrell Schmidt[3] telescope at the Kitt Peak National Observatory.[4] The images were taken with a 2048×2048 frontside-illuminated Tektronix CCD (S2KA) mounted at Newtonian focus. This setup provides a wide 69×69 arcmin field of view, with each 21 μm pixel imaging 2.03 arcsec of the sky. The gain was set to 2.5 e/ADU and the chip showed a readout noise of 3.0 electrons. All exposures were made through a Harris R band filter.

Observations were performed in a manner similar to MBH. Half the observing time was used to observe the galaxy, the other half to obtain a large number of dark sky flats for accurate flatfielding. In the case of NGC 891, alternating galaxy and dark sky exposures were taken at approximately the same hour angle and declination. Over the four photometric nights, a total of 45 galaxy frames and 45 sky flats were taken, each with an integration time of 600 s.

Overscan and bias subtraction were performed in the usual way, and dark frames were taken but found to be unnecessary. A "super sky flat" was constructed using the dark sky exposures. This process is described in detail in Appendix A. Estimated errors on the final flat field were an error over small scales (due to photon statistics in the dark sky flats) of 0.05%, and an error over larger scales ($\sim$100 pixels), due to intrinsic sky variations and residual stellar features in the sky flats, of 0.07%. These excellent results made accurate surface photometry possible for the galaxy.

Each separate galaxy exposure was divided by the normalized flat field and shifted to a common positional center using IRAF's[5] geomap/geotran routines. Each galaxy image was individually sky subtracted by subtracting its mode (correctly determined using our own code, since the IRAF mode calculation algorithm is inaccurate, see Appendix A) because the sky level varied from frame to frame. Then the sky-subtracted images were combined using a median.

Final sky subtraction on the combined galaxy image was accomplished in an iterative manner. First, the image was binned into 100×100 pixel bins and the sky level estimated by calculating the mode of each bin. Then a plane was fitted to these sky estimates, using only those parts of the image that were uncontaminated by galaxy light or bright stars. This plane (which varied from a constant by only 4 ADU or

[3]Observations were made with the Burrell Schmidt of the Warner and Swasey Observatory, Case Western Reserve University.

[4]Kitt Peak National Observatory (KPNO) is a division of the National Optical Astronomy Observatories (NOAO), which are operated by the Association of Universities for Research in Astronomy, Inc. (AURA) under cooperative agreement with the National Science Foundation.

[5]IRAF is distributed by the National Optical Astronomy Observatories, which are operated by the Association of Universities for Research in Astronomy, Inc., under cooperative agreement with the National Science Foundation.

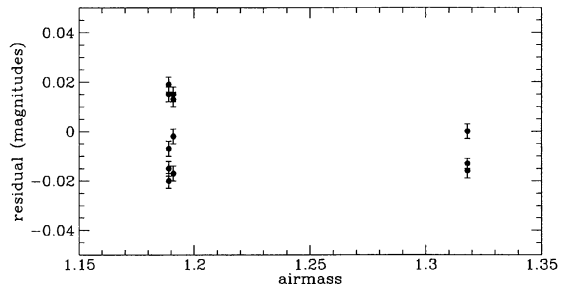

FIG. 2. Residuals of photometric standards from our calibration fit are shown as a function of airmass—all residuals are small, and no significant airmass term is seen.

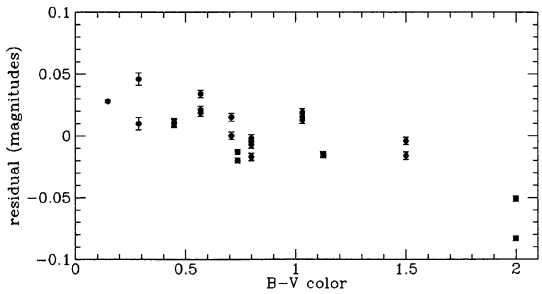

FIG. 3. Residuals from our photometric calibration are plotted as a function of $B-V$ color of the standard star. Since we observed only in one color (R) we are unable to correct for a color term in our calibration, but the above plot shows that such an effect is less than 0.10 mag over the whole likely range of stellar colors.

0.2% over the entire image) was then subtracted from the galaxy image. The second stage of sky subtraction was done when the mask for foreground stars and background galaxies was constructed (see Sec. *3.1*). The above process was repeated using the un-masked pixels only, resulting in the final sky-subtracted image. The mean sky level on the final image was 1878±1 ADU.

It can be seen in the masked image (Fig. 4) that the sky appears brighter in regions near bright stars. This is because our stellar profile, estimated using DAOPHOT (Stetson 1987), did not extend far enough to mask the outer wings of these bright stars. In the next paper in this series (Morrison *et al.* 1997a) we will model the stellar profile to large radius and improve the sky subtraction further. Since our major aim in this paper is to characterize the relatively bright (R=20–26 mag/sq. arcsec) regions where the thin and thick disk dominate, we do not require this level of accuracy in sky subtraction in this paper, and will limit our analysis here to $R<26$ mag/sq. arcsec.

To simplify analysis, the final image was rotated 24.8° clockwise so that the major axis of the galaxy was parallel to the x axis of the frame. This is a position angle of 24.8°, consistent, within the errors of CCD rotation with respect to the N-S axis, with the PA of 23° measured by Scoville *et al.* (1993).

Typically, two Landolt (1992) standard star fields were observed per night over a range of airmass. This gave nine suitable, well-exposed standard stars. A photometric zero point of $R=22.05\pm0.03$ mag per sq arcsec corresponding to 1 count per second per pixel was derived (see Fig. 2). For a 600 s exposure, this leads to a value of $R=29.01\pm0.03$ mag per sq. arcsec corresponding to 1 count per pixel. Since observations were made only in one color, there is no way of adding a color term to the calibration, but we estimated the possible error due to the lack of color term as follows. For the entire color range from $0.0\leqslant B-V\leqslant2.0$ the photometric zeropoint shifts by less than 0.10 mag (see Fig. 3). We chose to normalize the photometric calibration for $B-V\simeq1.0$, a typical color for old stellar populations.

The average sky brightness, 1878 ADU per pixel, was $R_{sky}=20.8$ mag per sq. arcsec. During perfectly photometric conditions, the sky brightness varied by 0.5 mag during the run (see Appendix A for further discussion).

3. ANALYSIS

A distance of 10 Mpc was assumed for NGC 891 (Ciardullo *et al.* 1991), which is derived from the planetary nebula luminosity function of the galaxy. Circumstantial support for this distance comes from the recent *HST* Cepheid distance of 9.3 Mpc to another galaxy in the same group as NGC 891, NGC 925 (Silbermann *et al.* 1996). 10 Mpc corresponds to 98.5 parsecs per 2.03 arcsec pixel in our image.

3.1 Masking

We needed to remove contributions from non-galaxy light in the image. This includes light from stars and background galaxies, as well as obscuration from NGC 891's dust lane. This part of the analysis closely follows the techniques described in MBH. We created a mask so that the galaxy's dust lane, foreground stars and background objects could be excluded from the fitting and analysis.

The dust lane of the galaxy can be seen clearly in Fig. 1. A dust mask was created by analyzing a strip 30 pixels in height (±1.5 kpc) running the length of the major axis. This strip was broken up into 30 pixel segments, and a contour plot of each segment was examined carefully. The points at which the galaxy light "turns over" and begins falling off into the dust lane, or where the light distribution was "lumpy" due to dust, were noted for each segment. The corresponding regions in the mask image were set to zero. The dust mask at its widest point obscures z heights of up to 1 kpc (2 thin disk scale heights).

Accurately masking out the foreground stars was crucial due to the low galactic latitude of NGC 891 ($b=-17$). The relatively crowded nature of this field can be seen clearly in Figs. 1 and 4 (Plate 40). The positions and magnitudes of all the stars in the frame were determined using DAOPHOT (Stetson 1987). To accurately measure stellar magnitudes in such a crowded field, point spread function (PSF) photometry was needed. The PSF was calculated using 10 bright, relatively isolated stars following the procedure outlined in Stetson (1987) until a clean PSF in a 15×15 pixel box was obtained. Thus the stellar wings were accurately defined out to 15 pixels (30 arcsec) in radius.

The final aim of this process was not the brightness measurement of all stars in the frame, but the construction of a

mask which accurately obliterates all foreground stars. The powerful PSF-fitting capacities of DAOPHOT were required both because of the crowded nature of the field and because an accurate stellar brightness estimate is needed to decide how far out to mask a given star. One of the factors which strongly affected our limiting magnitude was the amount of starlight we could mask out while still retaining enough of the image for accurate data analysis. Thus an accurate estimate of the stellar profile was vital. The PSF was used to produce a radial profile to determine the radius at which the brightness of a star of a given magnitude fell below a value of 2.0 ADU per pixel. All pixels within this radius were masked out in the final mask image. Note that this corresponds to ~0.1% of the average sky background level, or 28.3 R mag per sq. arcsec. (If a lower limit of 1 ADU was used for the mask, only ~30% of the original image remained unmasked; for 2 ADU ~40% of the image was still useable.)

The final step in the creation of the mask was to mask out background galaxies and undetected stars by hand. These features, as well as large diffraction spikes, were masked out using IRAF's imedit. Special attention was paid to regions with significant galaxy light, where the brightness variation was steep enough to have confused DAOPHOT's sky-fitting algorithm. The mask was multiplied by the final galaxy frame to create a masked galaxy image. A portion of this image, centered on the galaxy, is shown in Fig. 4 (Plate 40).

In order to bin the data to increase signal-to-noise (S/N) in the faint outer regions of the galaxy, we used the same algorithm as MBH. Because of the lower spatial resolution of the Burrell Schmidt compared to the KPNO 36″ (where MBH's data were taken) the strips used in the construction of profiles parallel to the minor axis were 40 pixels wide. Bin sizes in the z direction varied from 3 pixels (in the bright disk areas) to 39 pixels in the sky. Un-masked pixels in a given bin were combined in a robust fashion (using a 2.5σ clip in large bins to remove undetected outliers such as faint stars or background galaxies).

Figures 5 and 6 show the profiles parallel to the minor axis for each side of the galaxy. The error bars were derived using an error model similar to that used by MBH for their data. The error model, and the tests used to show its reliability, is described in detail in Appendix A. Dominant sources of error in the brighter regions of the galaxy are photon statistics and surface brightness fluctuations, while in the faint outer regions, the major contributions are large-scale flat fielding errors and spatial sky brightness variations.

4. RESULTS

In this section we will first consider two possible complications to our analysis (warping of the stellar disk and contamination of the R-band data by extraplanar Hα emission) and show that neither is a problem. Then we use simple one-dimensional modelling of the vertical profiles to draw some preliminary conclusions and to highlight the limitations of this method. We also compare our preliminary parameters for the NGC 891 thin and thick disk with those obtained by other workers.

4.1 Is the Stellar Disk Warped?

Some edge-on galaxies such as NGC 4565 and NGC 5907 show clear warping in H I (Sancisi 1976; Rupen 1991) and it has been shown (Battaner *et al.* 1990; MBH; Morrison *et al.* 1997b) that their disks also show a stellar warp in the outer regions. NGC 891's H I map shows little warping (Rupen 1991). We checked for a stellar warp in NGC 891 by folding each profile over its centerline and checking whether the position of these centers varied with radius. For purposes of comparison, note that NGC 5907 showed a variation of 15 pixels (or 600 pc) in the z-position of these centers from one end of its disk to the other. This effect was not visible at all in the NGC 891 image, where the centers were found to vary by no more than 1 pixel (98 pc) over the 450 pixel length of the major axis; the resulting angle of 0.1° is within our error for the frame rotation, so this variation is quite possibly a result of that. We conclude that this galaxy does not have a strong stellar warp. When we perform the full two-dimensional modelling of this galaxy (Morrison *et al.* 1997a) we will be able to test for a faint optical warp using residual images after models are fit and subtracted.

In Sec. 5 we will show that for galaxies with significant bulges, the outer disk regions are particularly important in determining the contribution of fainter stellar populations such as thick disk and halo. The lack of a warp in NGC 891 restricts the thin disk to an appropriately small region in the midplane and makes such investigations much simpler.

4.2 Hα Emission

The Harris R bandpass includes the Hα line, and since NGC 891 is known to have unusually strong diffuse extraplanar Hα emission, we need to check whether we will detect a significant amount of this emission, watered down in our much larger bandpass.

Dettmar (1990) and Rand & Kulkarni (1990) showed that the inner regions of NGC 891 have diffuse Hα emission at z distances up to 4.5 kpc. Typical values are EM=10 pc cm^{-6} at z=1 kpc and 2 pc cm^{-6} at z=3 kpc. Assuming a temperature of 10,000 K, we find a surface brightness of 1.5 $\times 10^{-17}$ ergs cm^{-2} sec^{-1} Å^{-1} deg^{-2} at z=1 kpc, or R=27.7 mag/sq. arcsec. The broadband surface brightness of the galaxy on the minor axis at this z height is R=21.0. Similarly, at z=3 kpc, we calculate a surface brightness of 3×10^{-18}ergs cm^{-2} sec^{-1} Å^{-1} deg^{-2}, or R= 29.4 mag/sq. arcsec, compared to the total galaxy surface brightness of R=23.5 on the minor axis. Thus the Hα contribution is some 6 magnitudes fainter than the observed R surface brightness, and can be safely neglected.

4.3 One-dimensional Modeling

We will begin with a simple one-dimensional approach to draw some basic conclusions and explore the limitations of this method.

The fits were made using a nonlinear least-squares technique and the Marquardt-Levenberg minimization algorithm

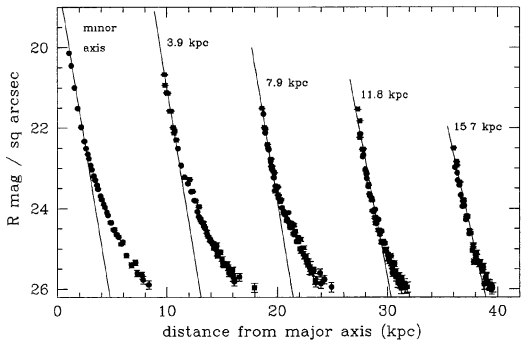

FIG. 5. Vertical profiles of NGC 891, with profiles above and below the plane, and from both sides of the galaxy center, superimposed. (Filled circles are from the RHS of the galaxy, filled squares from the LHS.) Also shown is our best one-disk fit to each profile. Such a fit is clearly unable to model low-z and high-z regions simultaneously—we need to add a second (thick) disk component to obtain an adequate fit.

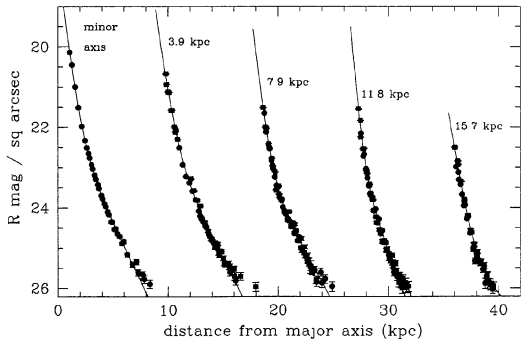

FIG. 6. Vertical profiles (as in Fig. 4) with our two-disk one-dimensional fits shown as solid lines. The large number of parameters used (many of which are highly correlated) produce unconstrained solutions such as surface brightnesses in the plane which do not decrease with radius.

of Press *et al.* (1992). Unlike the fits of MBH, in this case the fit data were the data points displayed in the profiles of Fig. 5 *in magnitudes*, rather than the linear counts from the CCD. (This logarithmic transformation, although it does not deal absolutely correctly with the error estimates, has the advantage of suppressing the sensitivity of the least-squares technique to outliers.) For these fits the galaxy was assumed to be perfectly edge-on so that the exponential scale heights found from the fits to the surface brightness data are equivalent to the scale heights of these populations in the three-dimensional galaxy.[6]

The first model fit to the data was a single exponential disk

$$m = m_1 - 2.5 \log(e^{-a_1|z|}).$$

Here m is the surface brightness in R magnitudes per sq. arcsec, z is the distance from the plane, m_1 is the surface brightness of the disk at the plane, and a_1 is the inverse scale height of the disk (in more familiar notation $a_1 = 1/h_{z1}$).

It is clear from Fig. 5 that a single exponential disk (a straight line in the surface brightness versus linear distance plot) does not fit any profile well—the gradient is steeper for points close to the plane, where the galaxy's thin disk dominates, and flattens at larger z, where the thick disk identified by van der Kruit & Searle (1981b) dominates. Figure 5 shows our best one-disk fits, where the disk scale height was allowed to vary for each profile, and illustrates this point clearly. We confirm the vdKS result that NGC 891 has a thick disk.

We then fit models with two exponential disks to the profiles:

$$m = m_1 - 2.5 \log(e^{-a_1|z|} + f e^{-a_2|z|}).$$

Here m and z are as before, m_1 is the surface brightness of the thin disk at the plane, a_1 and a_2 are inverse scale heights of thin and thick disk, respectively, and f is the ratio of thick to thin disk surface brightness at the plane. Each data point was weighted appropriately by its errors.

Note that we have not included two other possible luminosity components—bulge and halo—in this model. From examination of the image, it can be seen that most of the influence of the bulge should be confined to the minor axis profile, although the 3.9 kpc profile may also be affected. Using the properties of the Milky Way halo given in the next section to guide us, we have chosen to restrict our one-dimensional fits to the region where disk and thick disk would dominate (± 50 pixels from the plane, or approximately 5 kpc). The regions where the fit was made are marked by vertical lines in Fig. 7. This means that results from the one-dimensional fits may be biased (probably towards larger scale heights) by the non-inclusion of a halo component. However, we see in Fig. 8 (Plate 41) that the Milky Way halo is some 3 mag fainter than the outer disk of NGC 891 (where the thick disk dominates), so this may not be a problem.

The results of this fit, with estimates of correlation coefficients from the nonlinear least-squares formalism, are shown in Tables 1 and 2 and Fig. 6. With 5 profiles and 4 parameters fit to each profile, the galaxy luminosity distribution is currently being fit with 20 free parameters, an unnecessarily large number. The errors from the nonlinear least-squares formalism are not quoted—these formal errors are often orders of magnitude smaller than realistic estimates. We demonstrated in MBH by experiments with realistic fake data sets that nonlinear least-squares error estimates often have no global relevance, as they are determined only by the immediate neighborhood of the minimum. In the full two-dimensional analysis we will use a bootstrap error estimate which yields more realistic values.

The correlation coefficients between several parameters are dangerously high: for most profiles, disk normalization and scale height are almost perfectly correlated for both thin and thick disk, as are the two disk scale heights. Also, it can be seen in both Table 1 and Fig. 6 that the surface brightness on the major axis does not decrease monotonically with radius in these fits as we might expect (for example, see Fig. 6 of vdKS).

The effect of these high correlation coefficients can be seen graphically in Fig. 7. For both fits, scale heights of thick and thin disk were held constant and the other two param-

[6] Sancisi & Allen (1979) estimate an inclination of more than 87.5° for NGC 891, so this assumption is not a problem.

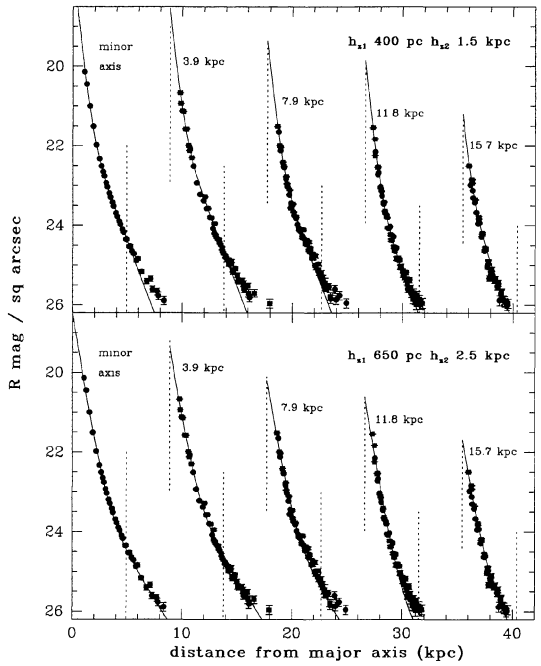

FIG. 7. This figure illustrates the non-unique nature of one-dimensional fits to averaged vertical profiles. Over the restricted z-range used for the fits (the region between the dotted lines) both combinations of thin and thick disk scale heights fit almost equally well.

eters allowed to vary: in the top panel the scale heights were 400 pc and 1.5 kpc, respectively, and in the bottom panel the scale heights were 650 pc and 2.5 kpc. By restricting the number of parameters to a more reasonable number, some of the undesirable properties of the first fits have been avoided (now the central surface brightnesses do fall with radius, as expected). However, over the range of z heights used, both models, whose parameters differ significantly, fit the profiles almost equally well.

Early fits to galaxy luminosity profiles (e.g., the disk/bulge decompositions of Boroson 1981) did not suffer from the problem of highly correlated parameters—it was possible to find regions of the image where the disk dominated and the bulge could be neglected, and vice versa. As we extend our analysis to fainter surface brightness values and thus include more stellar populations, it is more difficult to find regions where each component dominates. In the two-disk fits we have attempted, the dust mask (which extends to two thin disk scale heights in places) covers the region where the thin disk dominates, and our restriction to $\mu_R > 26$ mag/sq. arcsec means that we have only limited data on regions where the thick disk dominates, free from any thin disk domination.

Bahcall & Kylafis (1985) noted the covariance problem when they attempted to use this technique to fit the vdkS photographic data (which reaches to about $R=25$): "We found that an unrealistically large range of acceptable parameters was consistent with the observed z dependence." Also, Acton (1970) discusses the problems inherent in fitting two different exponential functions to a dataset. We conclude that in situations such as this where two or more stellar components contribute comparably to the profile, *one-dimensional fits to the vertical profiles should be viewed with caution.* There are two improvements that we will explore in the next paper—reaching yet fainter to increase the spatial range over which each population can be detected, and using the full two-dimensional fit to use the data more efficiently. (It can be seen from MBH's analysis of NGC 5907 that correlation coefficients are smaller with the two-dimensional analysis.)

TABLE 1. One-dimensional fits to NGC 891 profiles.

Profile	Minor axis	3.9 kpc	7.9 kpc	11.8 kpc	15.7 kpc
m_1 (R mag/sq. arcsec)	17.91	19.09	19.63	19.53	21.69
h_{z1} (kpc)	0.48	0.51	0.47	0.33	0.65
f	0.048	0.103	0.055	0.072	0.045
h_{z2} (kpc)	1.69	1.71	2.26	1.38	4.39

We have shown that in cases such as this where several stellar components overlap spatially, one-dimensional least-squares fitting to vertical profiles is not sufficiently powerful to separate the components in a unique fashion. The fact that 3 out of 6 correlation coefficients in Table 2 are close to 0.9 shows that this situation is extreme. It is not possible to obtain meaningful independent estimates of these parameters using this technique. Thus the best way to summarize the results of our fits is to quote ranges of parameters which provide acceptable fits. These are shown in Table 3.

Table 3 also shows the results of fits by three different groups (vdKS; Bahcall & Kylafis 1985; Shaw & Gilmore 1988) to the vdKS photographic F-band surface photometry. It can be seen that there is good agreement on the thin disk scale height. Since photographic zero points for surface photometry are notoriously hard to determine, due to the difficulty of "flat fielding" photographic plates, the difference in central surface brightness (m_1) values is not surprising.

It can be seen that agreement is less good for thick disk parameters. Our wide range of thick disk fraction includes both other estimates, but even though all others come from the same dataset, they still do not agree. The two two-dimensional fits fail to agree on thick disk scale height, as well. The vdKS photographic photometry goes faint enough to demonstrate the existence of the NGC 891 thick disk, but clearly is not of high enough S/N to make it easy to measure its parameters. Our data go significantly deeper, so our two-dimensional fits should constrain the thick disk parameters much better. Our thick disk scale height values are larger than the other two estimates; this probably reflects the fact that we detect the thick disk over a larger range of z and so measure its scale height more accurately, but may also be skewed by the omission of a halo component. However, it can be seen in Fig. 8 that NGC 891's halo would have to be several magnitudes brighter than the Milky Way's for this to be a problem.

TABLE 2. Correlation coefficients from one-dimensional fits to minor axis.

Parameter	h_{z1}	f	h_{z2}
m_1	−0.95	−0.52	−0.75
h_{z1}		0.73	0.89
f			0.95

TABLE 3. Parameter ranges from one-dimensional fits, compared to previous work and to Milky Way.

Source	Thin disk		Thick disk	
	m_1 (R mag/sq. arcsec) (Minor axis)	h_{z1} (pc)	f (all profiles)	h_{z2} (kpc)
NGC 891: this work	17.4–18.6	400–650	0.03–0.21	1.5–2.5
NGC 891: vdKS	19.3	500	Existence only	
NGC 891: BK (2D)		500	0.15–0.33	1.0–1.35
NGC 891: SG (2D)	19.05	540	0.10	1.76
Milky Way	18.0	350	0.02–0.10	1.0

5. DISCUSSION—COMPARISONS WITH THE MILKY WAY

It has been noted (van der Kruit 1984; Scoville *et al.* 1993) that our Galaxy and NGC 891 share many similarities. Thus it is useful to review the properties of the Milky Way's stellar populations (which are much better understood) to guide us in our investigation of the luminosity distribution of NGC 891. Most of the results discussed below are based on star counts or detailed studies of samples of individual stars—their space distribution, kinematics, metallicity, and age. This amount of detail makes it possible to go beyond taxonomy and begin to infer how and when the populations formed and evolved. In contrast, NGC 891 is sufficiently far away that individual stars cannot be resolved from the ground, and so only integrated properties of the stellar populations can be observed. Our observations are also taken through a broadband (R) filter. This means that in regions of the galaxy where more than one stellar population is present, far less information is available to help separate populations with different formation histories. We will use the Milky Way to alert us to possible complications in our interpretation of the NGC 891 data.

One criticism of stellar populations studies is that the populations discussed are merely convenient labels, useful groups to sort stars into, but do not correspond to different formation or evolutionary histories. We believe that there is now sufficient evidence to justify the divisions discussed below—the population in question *does* relate to a specific formation event or evolutionary history. The recent advances that have made this conclusion possible include more precise measurements of stellar age and kinematics. This is clearly much harder, if not impossible, for external galaxies, and highlights the importance of making a careful comparison between NGC 891 and the Milky Way, in the hope that the global view of the more distant galaxy will complement the detailed knowledge of our own.

Figure 8 (Plate 41) shows the Milky Way stellar populations in summary form, drawn as R-band surface brightness profiles seen viewing the Galaxy edge-on from outside. The assumptions that go into this model are summarized in Appendix B. The two least well-understood populations (thick disk and halo) are shown by two lines each, which cover the current uncertainty in their properties. The model becomes increasingly unrealistic for z distances below 300 parsecs, because dust and young stars make the profiles more complex close to the plane. (In reality, if the Milky Way were viewed from outside, dust obscuration would remove much of the R-band light at low z.)

The minor axis profile in Fig. 8 shows strong contributions from all four components (although it should be noted that the thick disk profile here is pure extrapolation, as this population has not been studied close to the Galaxy's center). Thus, although the minor axis might seem the most promising place to start because the galaxy is brightest there, it is actually the most difficult in terms of interpretation. In contrast, the outer disk profiles ($R \geq 8$ kpc) show clear regions where thin and thick disk and halo predominate. Unfortunately, this happens at low surface brightness levels for the thick disk and particularly the halo. The deep surface photometry techniques we have developed are vital for a real understanding of this complex topic in other galaxies.

Below we list each major stellar component of the Milky Way, summarize its properties, and compare it to the corresponding population in NGC 891.

5.1 Young Thin Disk

This includes young (O and B) stars and clusters, H II regions, molecular clouds and dust. In the Milky Way, such objects have a small vertical scale height of order 100 pc (Bahcall & Soniera 1980; hereafter BS; Mihalas & Binney 1982). Because the dust in an edge-on system like NGC 891 obscures so much of the starlight behind it, we have chosen to mask out regions with appreciable dust absorption in our R-band image, and thus we are unable to study this population. However, Scoville *et al.* (1993) have studied NGC 891's molecular gas in detail using CO aperture synthesis. They conclude that although its radial CO distribution is remarkably similar to the Milky Way's, its total molecular gas mass is more than twice the Galaxy's (despite a presumably similar total galaxy mass inferred from their similar rotation curves), and its vertical CO extent is *twice* that of the Galaxy's (a FWHM of 240 pc compared to 120 pc for the Milky Way). We will return to this in the next section, when discussing the thickness of the stellar disk.

The remaining discussion lists the other stellar populations in decreasing order of total luminosity in the Milky Way.

5.2 Old (Thin) Disk

Old disk stars in the Milky Way have ages of 1 Gyr and more, and have thus had time to become dynamically well

mixed and heated via secular evolution processes. These include scattering by spiral arms and giant molecular clouds which cause inhomogeneities in the disk potential (Spitzer & Schwarzschild 1951; Sellwood & Carlberg 1984; Jenkins & Binney 1990). The old disk contains most of the luminous mass of the Galaxy, with a total mass of $5\times10^{10}M_{\odot}$ (Kent *et al.* 1991). It has scale height of ~350 pc (BS; Gilmore & Reid 1983), a scale length of 3–5 kpc (van der Kruit 1986; Kent *et al.* 1991), and a maximum radius of approximately 20 kpc (Carney 1984). Its edge-on central surface brightness is $R=18.0$ mag/sq. arcsec.

The Milky Way thin disk edge-on central surface brightness ($R=18.0$) is within the range of our possible solutions for NGC 891's disk. Their disks have a similar radial extent. However, as is graphically illustrated in Fig. 8, where we have plotted the NGC 891 data on top of the Milky Way model, NGC 891 is significantly more extended vertically. Scale heights for both thin and thick disk are larger in NGC 891, despite the galaxies' presumably similar total masses. Our estimates of possible thin disk scale heights range from 400 to 650 pc, with all other workers estimating a scale height close to 500 pc, while the Milky Way old disk scale height is 300–350 pc. We discuss possible reasons for this difference below.

(i) Could this be caused by our masking out of NGC 891's dust lane, which means that we are unable to study the inner two scale heights of its thin disk? MBH considered this possibility for NGC 5907, where even more of the thin disk needed to be masked because of its lower inclination, and concluded that this was not a problem.

(ii) The disk scale height measurements for the Milky Way come from star counts and inferences from stellar kinematics. For NGC 891, the measurements come from integrated light—could the different measurement techniques bias the answers, meaning that we are trying to compare apples and oranges here? In fact, measurements of disk scale height in the Milky Way have been made using a similar method, by Kent *et al.* (1991), who used the Spacelab near-IR data to parameterize the Milky Way disk. His derived scale height was *smaller* than the star count values (250 pc). Because it is possible that the near-IR data have been contaminated by light from younger stars (Binney *et al.* 1996), we prefer to use the star count numbers here, and feel that because we have masked out low z values our scale height measurements for NGC 891's disk should not suffer contamination by young stars.

(iii) Another possibility is that the distance to NGC 891 has been over-estimated. However, its true distance would need to be reduced from 10 to ~6 Mpc to remove the discrepancy, which seems unlikely. The planetary nebulae detected by Ciardullo *et al.* (1991) would have to be approximately a magnitude fainter (and thus significantly older) than the M31 planetary nebulae with which the luminosity function measurements are calibrated, and we have no reason to expect such an enormous age difference between these stellar populations. Because NGC 891 is edge-on, it is not possible to measure its distance directly using Population I distance indicators such as Cepheids; but a distance measurement via the detection of the giant branch tip with *HST* (Lee *et al.* 1993) would be possible, although expensive in terms of telescope time.

(iv) The most likely explanation involves heating mechanisms for the old disk. Young stars in the Milky Way are formed with very small scale heights (of order 100 pc) and heated by scattering off large inhomogeneities in the disk potential caused by spiral arms and giant molecular clouds. The main *vertical* heating process is interaction with giant molecular clouds; this saturates at a scale height of 350 pc in the Galaxy because once stars are heated sufficiently to keep them out of reach of the giant molecular clouds for most of their orbits, no further heating can occur.

Scoville *et al.* (1993) present high-resolution CO observations of NGC 891, and show that while its radial distribution of molecular gas is very similar to the Milky Way's, its vertical CO extent is twice as large, and its molecular gas mass is more than twice the Milky Way's. The mass function of molecular clouds in the Milky Way is biased toward large masses (Scoville & Sanders 1987; Stutzki & Gusten 1990), so it is likely that these CO measurements give a good indication of the distribution of giant molecular clouds in NGC 891. (Scoville *et al.* suggest that the larger CO scale height in NGC 891 is unlikely to be because of a decreased mass density in the disk, and more likely to be caused by NGC 891's more intense star-forming activity and higher ISM mass. This intense star-forming activity is also reflected in its unusually strong extraplanar Hα emission.)

If the major population of scatterers of the old disk stars in NGC 891 is both more numerous and more spatially extended, it should be more effective at heating disk stars to larger z heights, and we would expect to see a kinematically hotter disk, if the underlying gravitational potential is the same. Gerssen *et al.* (1997) have studied this effect more directly in NGC 488 (an Sb galaxy of intermediate inclination) by measuring the shape of its velocity ellipsoid. They find, similarly, that the ratio of vertical to radial velocity dispersion of thin disk stars is higher in this galaxy than in the Milky Way, and note that NGC 488 has a higher mean CO surface density than the Milky Way, which should make molecular cloud heating more effective.

5.3 Bulge/Bar

Recent results on gas kinematics (Binney *et al.* 1991) and space-based near-IR photometry (Blitz & Spergel 1991; Weiland *et al.* 1994; Dwek *et al.* 1995; Binney *et al.* 1996) have forced a re-assessment of the classical concept of the Milky Way bulge, which was originally thought to be the inner metal-richer part of the stellar halo (Baade 1944). It has now been shown that the Galaxy has a bar which extends to a radius of 2–3 kpc, oriented so it is viewed almost end-on from the Sun. Its "vertical scale height" is of order 400 pc (Kent *et al.* 1991; Dwek *et al.* 1995)—in other words it is a bar with significant vertical extent. Its total mass is of order $10^{10}M_{\odot}$ (Kent *et al.* 1991; Kent 1992; Dwek *et al.* 1995). We probably do not need an extra "bulge" component in addition to the bar (Kuijken 1996), although there are some metal-poor, kinematically hot stars from the stellar halo in the central few kpc of the Galaxy (Walker & Terndrup 1991; Morrison & Harding 1993; Minniti 1994). Thus the central

few kpc of the Milky Way differ markedly from those in our more massive neighbor M31, whose bulge is clearly not a bar but a classical $r^{1/4}$ system (de Vaucouleurs 1958). Our bar is a distinct spatial component in the Galaxy, but its evolution must be closely tied to that of the inner disk. (We discuss M31's bulge in the context of bulge/halo connections below.)

The NGC 891 bulge has somewhat boxy isophotes, suggesting that it too could be a bar seen close to end-on. This has been suggested by Garcia-Burillo *et al.* (1992), on the basis of their CO observations, although these observations are not of high enough S/N or spatial resolution to be more than suggestive. It is also interesting to note the strong similarity in radial CO distribution between the Milky Way and NGC 891—most spirals show a continuous drop of CO with radius, while both these galaxies have nuclear CO peaks, a region with little CO emission, and then a ring (Scoville *et al.* 1993). Bars are efficient at channeling gas in towards their center, and the Milky Way bar has likely caused the empty region between the 3 kpc ring and the nucleus. Perhaps this has happened also in NGC 891.

The best way to decide conclusively about the nature of the NGC 891 bulge is via the kinematical technique of Kuijken & Merrifield (1995) which looks for signatures of orbit families only permitted in a triaxial potential, in a major axis spectrum. We plan to make these observations for NGC 891, as it is important to understand whether its bulge should be thought of as part of its "spheroid" or its inner disk.

5.4 Thick Disk

In the Milky Way, approximately 5% of the stars near the Sun belong to the thick disk—a rotationally supported component with scale height 1 kpc (see Majewski 1993 and MBH for a review of its properties). Its edge-on central surface brightness is $\sim R=22$ mag/sq. arcsec, and its mass is $\sim 7\times 10^9 M_\odot$, although this mass is not well constrained because most studies of the thick disk in the Milky Way have been confined to regions a few kpc from the Sun. Thick disk stars are the oldest, most metal-poor disk stars, and the kinematic discontinuity seen in the high quality data of Edvardsson *et al.* (1993) suggests a specific formation event for the thick disk, such as the accretion of a small satellite by the Milky Way. It can be seen from Fig. 8 that in the Milky Way, thin and thick disks contribute equal surface brightness at about 1.5 kpc above the plane (4–5 thin disk scale heights). At the solar radius and 1.5 kpc above the plane, each component has a surface brightness of $R=24.5$ mag/sq. arcsec.

The existence of NGC 891's thick disk has been demonstrated in the previous section—it is clearly visible in Fig. 1 and in the vertical profiles of Fig. 5. Our range of possible scale heights (1.5–2.5 kpc) is significantly larger than the 1 kpc scale height of the Milky Way thick disk. Because of their small scale heights, giant molecular clouds are unable to heat disk stars to scale heights of order kiloparsecs (Binney & Lacey 1988) and other heating methods need to be considered to explain the formation of a thick disk. The currently most attractive theory of thick disk formation (heating of the disk following a minor merger, Quinn & Goodman 1986; MBH) also may have some difficulty in producing disks with scale heights as large as 2 kpc (see, for example, the "live halo" simulations of Walker *et al.* 1996, which show that the halo carries away much of the orbital energy of the satellite). We badly need more n-body simulations of the ambitious size of the Walker *et al.* (1996) work so that the parameter space of minor mergers can be explored in more detail. Barnes (1996) shows that a 3:1 mass ratio merger effectively destroys the disk, and other workers consider 10:1 mass ratios—perhaps a 7:1 mass ratio merger would produce a thicker disk. It is also clear from the symmetry and smoothness of the NGC 891 thick disk that it was not created by a recent event, and has had sufficient time (of order several Gyr) to mix dynamically. This can be seen by comparing our Fig. 1 with Fig. 5 of Walker *et al.* (1996).

5.5 Stellar Halo

This is the most ethereal of the Galaxy's stellar populations, with a total mass of only $\sim 10^9 M_\odot$ (Preston *et al.* 1991; Suntzeff *et al.* 1991; Morrison 1996). Its stars are predominantly very old and metal-poor, suggesting an origin in the early history of the Milky Way, although there are some interesting exceptions to both properties (Preston *et al.* 1994; Carney *et al.* 1996) which suggest a more complex history. The stellar halo is roughly spherical, with a mild flattening of $b/a=0.6$ near the Sun (Hartwick 1987; Preston *et al.* 1991) and has zero or retrograde net rotation (Norris 1986; Majewski 1992, and references therein). It is extremely centrally concentrated, with a radial density profile of $r^{-3.5}$ (Zinn 1985). There are about 800 disk stars to every halo star near the Sun (Bahcall & Casertano 1986; Preston *et al.* 1991; Morrison 1993), making the identification of Milky Way halo stars a challenging observational undertaking. Thick disk and halo contribute equal surface brightness at $R=8$ kpc, $z=5$ kpc; this happens at a surface brightness of 27.5 R magnitudes/sq. arcsec.

As we only examine data reaching to $R=26$ mag/sq. arcsec in this paper, we are unlikely to detect NGC 891's stellar halo if it is similar to the Milky Way's (except perhaps on the minor axis where strong contributions from thin disk, thick disk and bulge will make interpretation very difficult). However, the M31 halo is significantly brighter than the Milky Way's along its minor axis at distances of 10–20 kpc (Pritchet & van den Bergh 1994), so if NGC 891's halo more closely resembled M31's, it would be easier to detect. Unlike the Milky Way, M31's bulge light smoothly follows an $r^{1/4}$ law along the minor axis from 2–20 kpc, so the distinction between bulge and halo is less clear. Freeman (1996) discusses ways of distinguishing between bulge and halo using kinematical data—we will return to the interesting question of bulge-halo connections in a future paper.

6. CONCLUSIONS

We have performed deep CCD surface photometry of the nearby edge-on spiral NGC 891. In this paper we present data to $R=26$ mag/sq. arcsec, ~ 1 mag fainter than the best photographic work. NGC 891 is a particularly interesting galaxy because of its close resemblance to the Milky Way.

We have demonstrated that it lacks a stellar warp in the outer disk, which makes it a good candidate for study of thick disk and halo. However, its low galactic latitude ($b=-17°$) makes it difficult to study because of the large number of foreground stars. We have used PSF-fitting photometry to construct a mask for these stars which allows reliable elimination of contamination to $R=26$ mag/sq. arcsec in the stellar profiles. In a subsequent paper (Morrison *et al.* 1997a) we plan to use more sophisticated techniques to go significantly fainter.

We calculate that the unusually strong diffuse extraplanar Hα emission seen in NGC 891 at distances of up to 4.5 kpc (Dettmar 1990; Rand & Kulkarni 1990) does not contribute significantly to our broadband R surface photometry. At $z=1$–3 kpc, we find that the Hα emission, diluted in the broad R passband, is 6 mag or more fainter than the total galaxy brightness, and therefore can be safely neglected.

Before embarking on the full two-dimensional fit of this complex system, we investigate the usefulness of fitting averaged profiles perpendicular to the minor axis with simple one- or two-disk models. This technique clearly shows the need for a second (thick) disk to fit the luminosity profiles at $z>1$ kpc, but is unable to provide a unique best fit for the two-disk model because of very strong correlations between parameters. The range of permissible parameters for thin and thick disk scale heights from these fits is from 400–650 pc and 1.5–2.5 kpc for the thin and thick disks respectively. This problem with one-dimensional fits to vertical profiles was pointed out in 1985 by Bahcall & Kylafis, but the technique is still used extensively in analysis of present-day surface photometry (see, for example, de Grijs & van der Kruit 1996; Chen *et al.* 1997). When several stellar components overlap, a two-dimensional analysis is needed to reduce parameter correlations and produce more meaningful results. Our range of possible disk parameters is in good agreement with previous estimates of thin disk scale height.

We strongly confirm the result of vdKS that NGC 891 has a thick disk, and note that its luminosity distribution is quite smooth and symmetrical, suggesting that the stellar component has had time to become dynamically well mixed. Since our data go more than a magnitude fainter than previous photographic data, it is not surprising that our thick disk parameters do not agree well with previous work—we detect this component over a much larger region of the galaxy. The other two analyses of the vdKS data (Bahcall & Kylafis 1985 and Shaw & Gilmore 1989) fail to agree on either thick disk normalization or scale height; our large range of possible thick disk normalizations includes both their estimates, but the Bahcall & Kylafis (1985) thick disk scale height is smaller than our lower limit.

Comparing NGC 891 with the Milky Way, we find that both galaxies have similar thin disk central surface brightness and maximum disk radius, but that the scale heights of both thin and thick disk in NGC 891 are significantly larger than in the Milky Way. We explore possible reasons for this, and suggest that the larger thin disk scale height may be due to more effective heating by NGC 891's more massive and thicker molecular cloud layer.

It is a pleasure to thank Greg Aldering and Betsy Green for helpful conversations about sky brightness variations and Rob Kennicutt for help with the emission measure to R band surface brightness conversion. Also, we had illuminating discussions with Nick Scoville, Jeff Kenney, and Richard Larson about molecular cloud properties and with Chris Mihos about thick disks. H.L.M. and P.H. would like to thank the Oberlin College Physics department for their hospitality while the first draft of this paper was written. This work was supported in part by grants AST-9624542 to H.L.M., AST-9317605 to D.R.S. and AST-9421145 to Robert Kennicutt from the National Science Foundation.

APPENDIX A. DEEP CCD SURFACE PHOTOMETRY

A.1 Problems

There are several tough problems that need to be addressed in order to perform extremely deep surface photometry. These include a very low signal strength, the need to characterize the detector and telescope response extremely accurately, variable sky brightness and scattered light.

A.1.1 Signal strength

The signal we are measuring is $\ll 1\%$ of sky brightness. This means that estimating the background sky level correctly is paramount. Particularly at long wavelengths, the sky brightness can vary both temporally and spatially due to photochemical reactions in the upper atmosphere (see Herse *et al.* 1989 for some wide-field images). Thus it is important to measure background sky brightness at the same time as the object. This means that we need a field size significantly larger than the galaxy to be studied. The Burrell Schmidt's 1 sq. degree field, or the 24-arcmin CCD field of the KPNO 36″ are both well suited to this, and the Burrell Schmidt is ideal for large galaxies such as NGC 891. Figure 9 shows the entire CCD field used in our observations.

A.1.2 Detector and telescope response

It is important to characterize the response of the detector/telescope system very accurately—our inability to do this perfectly on large (>100 pixel) scales produces one of the fundamental limits to accuracy of the surface photometry. Extremely good flat fielding is needed.

Twilight flats provide a light source which is uniform only to $\sim 1\%$. This is accurate enough for many CCD imaging applications, but not for deep surface photometry. (A 1% flat-fielding error would cause a 100% error at an R surface brightness of 26 mag/sq. arcsec.) Also, the twilight sky is much bluer than a typical old stellar population, and since CCD response varies with wavelength, the use of twilight flats adds another source of error.

The best option is to take many dark sky flats, dithering exposures by a sufficient distance (of order arcminutes) so that not even the outer wings of stars overlap. The dark sky flats should be combined using a method optimized to remove all but background sky pixels (our experiments have shown that the IRAF CCDCLIP routine does a very good job with a large number of sky flats; we describe its application in more detail in the next section).

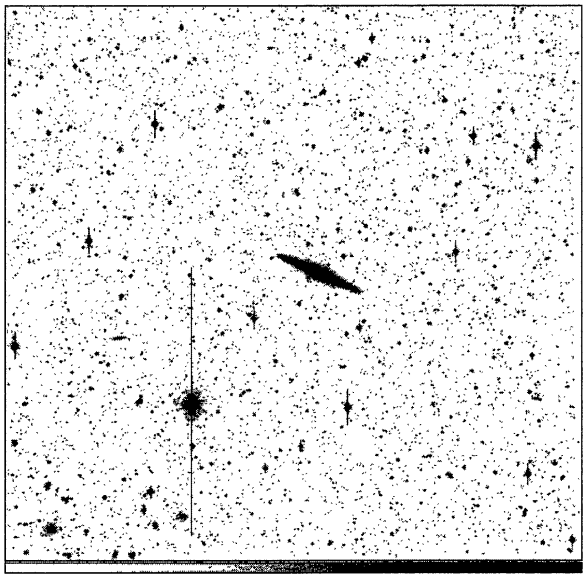

FIG. 9. The full Schmidt image of NGC 891. The 70′ square Schmidt field provides good regions for sky subtraction from the image itself, important for deep surface photometry. North is to the right, East down.

An additional safeguard is to take the sky flats at approximately the same telescope position (hour angle and declination) as the galaxy exposures. This means that any possible errors due, say, to slight shifts in telescope vignetting profile as a function of position or actual long-lived sky brightness gradients will cancel out. (In fact we have not detected any change of vignetting profile with position while using the Burrell Schmidt.) Ideally, we would work in the infrared mode where adjacent images are sky-subtracted before flat-fielding, but sky variations are on too short a timescale to make this practicable with CCD readout times of order several minutes.

A.1.3 Variable sky brightness

In the R-band, sky brightness occasionally varies because of airglow effects in the upper atmosphere, although at other times it stays quite constant.

Variable sky brightness can cause problems in two ways. If the sky is spatially as well as temporally variable (which we would expect on scales of order 1 degree because of the emission mechanism; see Herse *et al.* 1989 and Morrison *et al.* 1997b) it means that even dark sky flats are not uniform sources of illumination. Also, the sky subtraction of the galaxy image will be complicated by a patchy rather than an evenly varying sky.

In both of these cases, the only effective solution we have discovered (but see Chen *et al.* 1997) is to take a large number of sky and galaxy exposures (n of order 100) and average. The sky variations are uncorrelated, so any remaining uneveness in the background sky will be reduced by $\sqrt{n}$.

A.1.4 Scattered light

Scattered light is of particular concern in the detection of very faint extended sources, particularly if the object itself has a bright nucleus.

The best solution is, first, to use an observational setup which minimizes scattered light. This includes squeaky clean optics, good telescope baffling, masking of shiny objects near the light path and no re-imaging optics. The Burrell Schmidt is a good choice here because it is essentially impossible for light to reach the CCD other than by the "approved" path via the primary and newtonian flat. Its solid tube and internal ring girder construction prevent any light reaching the detector from outside the field being imaged.

Second, it is important to work hard in the analysis stage to characterize what scattered light still remains, by measuring the stellar PSF accurately to large radius and deconvolving the final image with this PSF as a check. (MBH describe this process in their Sec. *3.3.4.*)

A.2 Construction of Super-Sky Flat

In most observations taken in the R band, the mean sky brightness level does not vary appreciably. However, occasionally the airglow activity is so intense that sky variations more typical of the I band are observed. (In extreme cases the R band sky variations can be larger than I band variations, Green 1995.) In the October/November Schmidt run, we observed R sky brightness variations of order 50% for the entire run, with sky brightness ranging from $R=20.5$ to $R=21.0$ mag/sq. arcsec.

This meant that pre-scaling of the dark sky flats before combining them was particularly important, and that the averaging of a large number of sky flats was necessary to remove any spatial variations in sky brightness over the CCD. We chose to pre-scale by the mode of the image, which gives a robust estimate of the mean sky level. Because IRAF's mode calculation algorithm gives inaccurate results, we wrote our own routine to calculate the mode. IRAF's routine is inaccurate due to its inability to find the global maximum of the data histogram, particularly in the case (typical of most CCD data) where ADC conversion inaccuracies lead to slight biases in data values at 2^n boundaries.

The major drawback of using dark sky flats is the low flux level. Thus many sky flats must be combined to create a "super sky flat" with no leftover star features and a high signal-to-noise ratio. Forty-five sky flats were taken over the four night run. The flats were taken throughout the night in regions near to the galaxy so that they would accurately reflect the background brightness level and variation observed in the galaxy frames themselves. Between sky flats in the same region, the telescope was "dithered" by of order 10 arcminutes. This technique prevents the wings of bright stars from overlapping in the stack of flats.

An iterative procedure was used to produce the super sky flat. First, each sky flat was inspected for scattered light and extremely bright stars or clusters of stars. One sky frame was found to be undesirable and was rejected, leaving a total of 44 acceptable frames. Next, each sky flat was scaled by its mode. Finally, the sky flats were combined using a rejection algorithm (IRAF's CCDCLIP) that calculated the expected standard deviation in sky values from the CCD noise parameters and removed values more than 2σ from the median.

Each of the sky flats was divided by this super sky flat, significantly reducing the width of the distribution of sky

values, which gives a more accurate mode, and the modes of these flattened frames were determined. The entire procedure was repeated, with the original sky flats now being scaled by the new modal values. This procedure was repeated until no improvement was observed in the final super sky flat.

Each of the 45 galaxy images were flattened by the final super sky flat, then inspected to make sure they had no unwanted features such as strong scattered light (due to a bright star falling on the polished brass CCD mount in the dewar). The galaxy frames were corrected for first-order extinction, using the standard value of 0.10 for the R band.

A.3 Error Model

The error in our calculated brightnesses was modeled theoretically using to full advantage the well-defined noise parameters of the CCD. The sources of error in our data are similar to those identified by MBH, and since we followed the same basic reduction procedure, the error propagation is correspondingly similar.

A.3.1 Readout noise

For the CCD used in these observations, readout noise per pixel was 3.0 electrons, or 1.2 ADU. Since we median-combined 45 frames to obtain the final galaxy image, the noise was reduced by a factor of $1.22/\sqrt{45}$ to 0.22 ADU per pixel.

A.3.2 Photon noise

A pixel with a brightness of C ADU registered gC photons when exposed to light, giving rise to photon Poisson noise of $\sqrt{gC}$, or $\sqrt{C/g}$ ADU. Once again, this noise was reduced by image combination to $1.22\sqrt{C/45g}$, or $0.115\sqrt{C}$ ADU per pixel in the final image. An average sky pixel had a value of 1878 ADU, giving rise to a typical photon noise in the sky of 5.0 ADU, or 0.2%.

A.3.3 Small-scale flatfielding errors

Small pixel-to-pixel errors were introduced into the final image when each galaxy frame was flattened by the super sky flat. These variations arise from photon noise in the individual sky exposures. The total error per pixel in the final galaxy frame due to this effect is given by

$$\sigma_{\rm sff}=\frac{\sqrt{C_{\rm sky}}}{\sqrt{g}}\left(\frac{1.22}{\sqrt{n_{\rm flat}}}\right)\left(\frac{1.22}{\sqrt{n_{\rm gal}}}\right), \qquad \text{(A1)}$$

where $C_{\rm sky}$ is the mean sky background for a typical sky flat, g is the gain, $n_{\rm flat}$ is the number of combined sky flats, and $n_{\rm gal}$ is the number of combined galaxy frames. The first factor in Eq. (A1) is the fractional error of a single sky flat due to photon noise; the average sky value of 1878 ADU gives rise to a photon noise of 27.4 ADU, or 1.5%. The second factor comes from combining $n_{\rm flat}$ sky flats to create the super sky flat. The third factor arises from the fact that we combined $n_{\rm gal}$ galaxy images, each with slightly different positioning in the frame and hence independent errors.

With a sky flat photon noise of 1.5%, combining 44 sky flats and 45 galaxy frames gives us $\sigma_{\rm sff}=0.05\%$, a very small fractional error.

A.3.4 Large-scale flatfielding errors

Large-scale errors in the flatfielding are due to two dominant contributions: the variation of the sky brightness across an image and contamination from the wings of stars in the individual sky flats. When these flats were combined, the large-scale variations are reduced.

Because we had a large number of dark sky flats, it was possible to estimate directly the flatfielding error over large scales by making two independent sub-samples of sky flats (each containing 22 images; divided halfway through the run), constructing a super sky flat from each sub-sample, and comparing the two independent super sky flats. This was done by dividing the two super sky flats, using IRAF's BLKAVG to bin the divided image into bins of size 100×100 pixels (to remove variation due to photon statistics) and calculating the standard deviation of these bins. This was 0.21% of the mean value. Compensating for the fact that the final super sky flat was made with 44 images reduced the estimated error by another factor of $1/\sqrt{(2)}$, and the division of two images meant a reduction by another factor of 1/2.[7] Thus our final estimate of the large-scale flat-fielding error was 0.07%.

This is again a small fractional error. However, unlike the previously considered sources of error this effect is not diminished by increasing the number of pixels in a bin. This is one limiting factor on how well we can model the galaxy light at faint levels.

A.3.5 Sky background variations

We have seen that the sky background varied considerably from frame to frame, and within a frame. We need to estimate the error caused by spatial variations in sky brightness in the combined galaxy image.

Good regions of sky in the final masked galaxy image were identified, and the mean sky brightness was measured in bins of 100×100 pixels using the algorithm described in Sec. 2 to provide a robust average. The standard deviation of the 43 sky bins used was 1.63 ADU, with a mean sky level of 1878 ADU. This variation is caused both by large-scale flat-fielding errors (0.07% or 1.31 ADU) and by sky variation in the galaxy images. Subtracting quadratically we find that the sky variations contribute 0.97 ADU (0.05%) on large scales. This error, like the large-scale flat-fielding error, is not reduced by averaging large numbers of pixels so it gives another limit to the ultimate precision of our surface photometry.

A.3.6 Surface brightness variations

Another source of error comes from the intrinsic surface brightness variations of the galaxy. Since the light we are observing comes from individual stars in the galaxy and each pixel contains a finite number of stars, its value is subject to counting statistics. The variance of brightness fluctuations is characterized by Tonry & Schneider (1988). Following

[7]The traditional approximation that if two numbers are divided, the percentage error on their quotient is the sum of their individual percentage errors was checked by using Monte Carlo simulations and found to be a good approximation here.

MBH, we used values of $t=600$ s, $d=10^7$ pc, $\bar{M}=0$ for the R band, and $m_1=22.05$ mag/sq. arcsec. Then the variance of fluctuations due to surface brightness, σ_L^2, was $0.39\bar{g}$, where $\bar{g}$ is the mean number of counts due to the galaxy only. The effect of seeing was modelled empirically, as in MBH.

A.3.7 Sky level determination

In Sec. 4 we note that our error in sky level determination is 1 ADU, which corresponds to a magnitude of $R=29$ mag/sq. arcsec. Thus for the surface brightness levels considered in this paper, the error caused by sky level determination is entirely negligible.

APPENDIX B: MILKY WAY MODEL

We have constructed a luminosity model of our Galaxy which includes contributions from stars in the old (thin) disk, the thick disk and the halo. Since the bar/bulge is centrally concentrated enough to dominate all other populations close to the plane on the minor axis, we do not need to use galaxy models and have used surface photometry observations directly to describe this component on the minor axis.

The model is intended to summarize our current knowledge of the Galaxy's older stellar populations (with ages more than a few Gyr), and no attempt has been made to model the effect of young stars or dust. Thus the model becomes increasingly unrealistic for z heights of 350 pc and below. Since our purpose in compiling these data is to make comparisons with our NGC 891 surface photometry, where we have masked out regions close to the plane, this limitation is not of concern.

We have produced vertical profiles of the Milky Way, viewed from outside edge-on, at cylindrical distances from the galactic center of 0, 4, 8, and 12 kpc, to correspond to our NGC 891 profiles (the slight differences in radial distances are well within the uncertainties of our assumed value of $R_0=8$ kpc and the distance to NGC 891). The absolute magnitude of the Sun was assumed to be $M_R=4.31$ (Allen 1973).

The profiles are shown in Fig. 8 (Plate 41).

B.1 Thin Disk

The luminosity distribution of the old (thin) disk is assumed to vary exponentially with radius and z, with scale height 300 pc (Gilmore & Reid 1983) and scale length 3.5 kpc (BS; note that this value is also close to the more recent determination of Kent *et al.* 1991). Its luminosity density in the solar neighborhood was assumed to be $1.6\times10^7 L_\odot/\mathrm{kpc}^3$. This value was derived from a mass density of $0.044 M_\odot/\mathrm{kpc}^3$ (Luyten 1968), assuming a M/L ratio of 2.5, typical of old populations. (Note that the local *luminosity* density is much higher than this because it is dominated by younger stars such as A dwarfs—see Mihalas & Binney 1982 for discussion.) The maximum radius of the disk was assumed to be 20 kpc (Carney 1984).

B.2 Thick Disk

The local number density of the thick disk is still not well constrained, with published values ranging from $n_{\mathrm{thick}}/n_{\mathrm{thin}}=0.02$ (Gilmore & Reid 1983) to $n_{\mathrm{thick}}/n_{\mathrm{thin}}=0.09$ (Sandage 1987). Derived scale heights tend to be inversely proportional to the local density, and we have chosen values of 1.5 and 1.0 kpc, respectively, to cover the currently popular values (see MBH for a discussion). In the absence of any significant observational constraints on thick disk scale length or maximum radius, we have assumed that these parameters are the same as for the thin disk (3.5 kpc and 20 kpc, respectively).

B.3 Halo

The local luminosity density of halo stars was assumed to be $2.23\times10^4 L_\odot/\mathrm{kpc}^3$ (Preston *et al.* 1991). We have assumed two values for the power-law density profile exponent (-3.0 and -3.5, Saha 1985; Zinn 1985) and for the axial ratio b/a (0.6 and 1.0).

B.4 Bar/bulge

Because the Galaxy's bar/bulge dominates its surface brightness for $z<1$ kpc on the minor axis, and is sufficiently compact to contribute only to the minor axis profile in Fig. 8, we do not need to depend on bulge models, but have used the K-band minor axis profile of Kent *et al.* (1991). We transformed this to the R band assuming a typical bulge color of $R-K=2.3$ (de Jong & van der Kruit 1994), and joined this minor axis profile smoothly onto our model profile above $z=1.5$ kpc.

B.5 Caveats

Because we live in the middle of our Galaxy's disk, we can derive *local* volume densities of all the above components with reasonable accuracy. However, little observational work has been done on the nature of the thick disk and halo close to the galactic center, and so the predictions of the model for these components on the minor axis should be viewed with some caution.

REFERENCES

Acton, F. S. 1970, Numerical Methods That Work (Harper and Row, New York), p. 252

Allen, C. W. 1973, Astrophysical Quantities, 3rd ed. (Athlone, London)

Baade, W. 1944, ApJ, 100, 137

Bahcall, J. N., & Casertano, S. 1986, ApJ, 308, 347

Bahcall, J. N., & Kylafis, N. D. 1985, ApJ, 288, 252

Bahcall, J. N., & Soniera, R. M. 1980, ApJS, 44, 73 BS

Barnes, J. E. 1996, Formation of the Galactic Halo...Inside and Out, ASP Conf. Ser. 92, edited by H. Morrison and A. Sarajedini (ASP, San Francisco)

Battaner, E., Florido, E., & Sanchez-Saavedra, M. L. 1990, A&A, 236, 1

Binney, J., Gerhard, O., Stark, A., Bally, J., & Uchida, K. 1991, MNRAS, 252, 210

Binney, J., Gerhard, O., & Spergel, D. 1996, submitted to MNRAS

Binney, J., & Lacey, C. 1988, MNRAS, 230, 597

Blitz, L., & Spergel, D. 1991, ApJ, 379, 631

Boroson, T. A. 1981, ApJS, 46, 177
Burstein, D. 1979, ApJ, 234, 829
Carney, B. W. 1984, PASP, 96, 841
Carney, B. W., Laird, J., Latham, D., & Aguilar, L. 1996, AJ, 112, 668
Carney, B. W., Latham, D. W., & Laird, J. B. 1989, AJ, 97, 423
Chen, *et al.* 1997, submitted to AJ
Ciardullo, R., Jacoby, G., & Harris, W. 1991, ApJ, 383, 487
de Grijs, R., & van der Kruit, P. 1996, A&AS, 117, 19
DeJong, R. S., & van der Kruit, P. C. 1994, A&AS, 106, 451
de Vaucouleurs, G. 1958, ApJ, 128, 415
Dettmar, R-J. 1990, A&A, 232, L15
Dwek, E., *et al.* 1995, ApJ, 445, 716
Edvardsson, B., Anderson, J., Gustafsson, B., Lambert, D. L., Nissen, P. E., & Tomkin, J. 1993, A&A, 275, 101
Freeman, K. C. 1996, in Formation of the Galactic Halo...Inside and Out, ASP Conf. Ser. 92, edited by H. Morrison and A. Sarajedini (ASP, San Francisco)
Garcia-Burillo, S., Guelin, M., Cernicharo, J., & Dahlem, M. 1992, A&A, 266, 21
Gerssen, J., Kuijken, K., & Merrifield, M. R. 1997, submitted to MNRAS
Gilmore, G., & Reid, I. N. 1983, MNRAS, 202, 1025
Green, E. M. 1995, private communication
Hartwick, F. D. A. 1987, in The Galaxy, edited by G. Gilmore and R. Carswell (Reidel, Dordrecht)
Herse, M., Thuillier, G., Camman, G., Chevassut, J., & Fehrenbach, M. 1989, Appl. Opt., 28, 3944
Jenkins, A., & Binney, J. 1990, MNRAS, 245, 305
Kent, S. M. 1992, ApJ, 387, 181
Kent, S. M., Dame, T. M., & Fazio, G. 1991, ApJ, 378, 131
Kuijken, K. 1996, in Unsolved Problems of the Milky Way, IAU Symposium 169, edited by L. Blitz and P. Teuben (Kluwer, Dordrecht)
Kuijken, K., & Merrifield, M. 1995, ApJ, 443, L13
Landolt, A. U. 1992, AJ, 104, 340
Lanzetta, K. M., Bowen, D. V., Tytler, D., & Webb, J. K. 1995, ApJ, 442, 538
Lee, M-G., Freedman, W. L., & Madore, B. F. 1993, ApJ, 417, 553
Luyten, W. 1968, MNRAS, 139, 221
Majewski, S. R. 1992, ApJS, 78, 87
Majewski, S. 1993, ARA&A, 31, 575
Mihalas, D., & Binney, J. 1982, Galactic Astronomy (Freeman, New York)
Minniti, D. 1994, PASP, 106, 813
Morris, S. L., Weymann, R. J., Dressler, A., McCarthy, P. J., Smith, B. A., Terrile, R. J., Giovanelli, R., & Irwin, M. 1993, ApJ, 419, 524
Morrison, H. L. 1993, AJ, 106, 578
Morrison, H. L. 1996, in The Formation of the Galactic Halo, Inside and Out, ASP Conf. Ser. 92, edited by H. Morrison and A. Sarajedini (ASP, San Francisco)
Morrison, H. L., Boroson, T. A., & Harding, P. 1994, AJ, 108, 1191 (MBH)
Morrison, H. L., & Harding, P. 1993, PASP, 105, 977
Morrison, H. L., Harding, P., & Boroson, T. A. 1997b, in preparation
Morrison, H. L., Miller, E. D., Harding, P., Stinebring, D. R., & Boroson, T. A. 1997a, in preparation
Norris, J. E. 1986, ApJS, 61, 667
Press, W. H., Teukolsky, S. A., Vetterling, W. T., & Flannery, B. P. 1992, Numerical Recipes in Fortran, 2nd ed. (Cambridge University Press, Cambridge)
Preston, G., Shectman, S., & Beers, T. 1991, ApJ, 375, 121
Preston, G. W., Beers, T. C., & Shechtman, S. A. 1994, AJ, 108, 538
Pritchet, C. J., & van den Bergh, S. 1994, AJ, 107, 130
Quinn, P. J., & Goodman, J. 1986, ApJ, 309, 472
Rand, R., & Kulkarni, S. 1990, ApJ, 352, L1
Rupen, M. P. 1991, AJ, 102, 48
Saha, A. 1985, ApJ, 289, 310
Sancisi, R. 1976, A&A, 53, 159
Sancisi, R., & Allen, R. J. 1979, A&A, 74, 73
Sandage, A. 1987, AJ, 93, 610
Scoville, N. Z., & Sanders, D. B. 1987, in Interstellar Processes, edited by D. J. Hollenbach and H. A. Thronson (Reidel, Dordrecht), p. 21
Scoville, N. Z., Thakkar, D., Carlstrom, J. E., & Sargent, A. I. 1993, ApJ, 404, L59
Sellwood, J. A., & Carlberg, R. G. 1984, ApJ, 282, 61
Shaw, M., & Gilmore, G. 1989, MNRAS, 237, 903
Silbermann, N. A., *et al.* 1996, ApJ, 470, 1
Spitzer, L., & Schwarzschild, M. 1951, ApJ, 114, 385
Steidel, C. C., Giavalisco, M., Pettini, M., Dickinson, M., & Adelberger, K. L. 1996, ApJ, 462, L17
Stetson, P. B. 1987, PASP, 99, 191
Stutzki, J., & Gusten, R. 1990, ApJ, 356, 513
Suntzeff, N., Kinman, T., & Kraft, R. 1991, AJ, 102, 1118
Tonny, J., & Schneider, D. P. 1988, AJ, 96, 807
Tsikoudi, V. 1977, University of Texas Publ. Astron. No. 10
van der Kruit, P. C. 1984, A&A, 140, 470
van der Kruit, P. C. 1986, A&A, 157, 230
van der Kruit, P. C., & Searle, L. 1981a, A&A, 95, 105
van der Kruit, P. C., & Searle, L. 1981b, A&A, 95, 116 (vdKS)
van der Kruit, P. C., & Searle, L. 1982, A&A, 110, 61
Walker, A., & Terndrup, D. 1991, ApJ, 378, 119
Walker, I. R., Mihos, J. C., & Hernquist, L. 1996, ApJ, 460, 121
Weiland, J. L., *et al.* 1994, ApJ, 425, L81
Zinn, R. 1985, ApJ, 293, 424

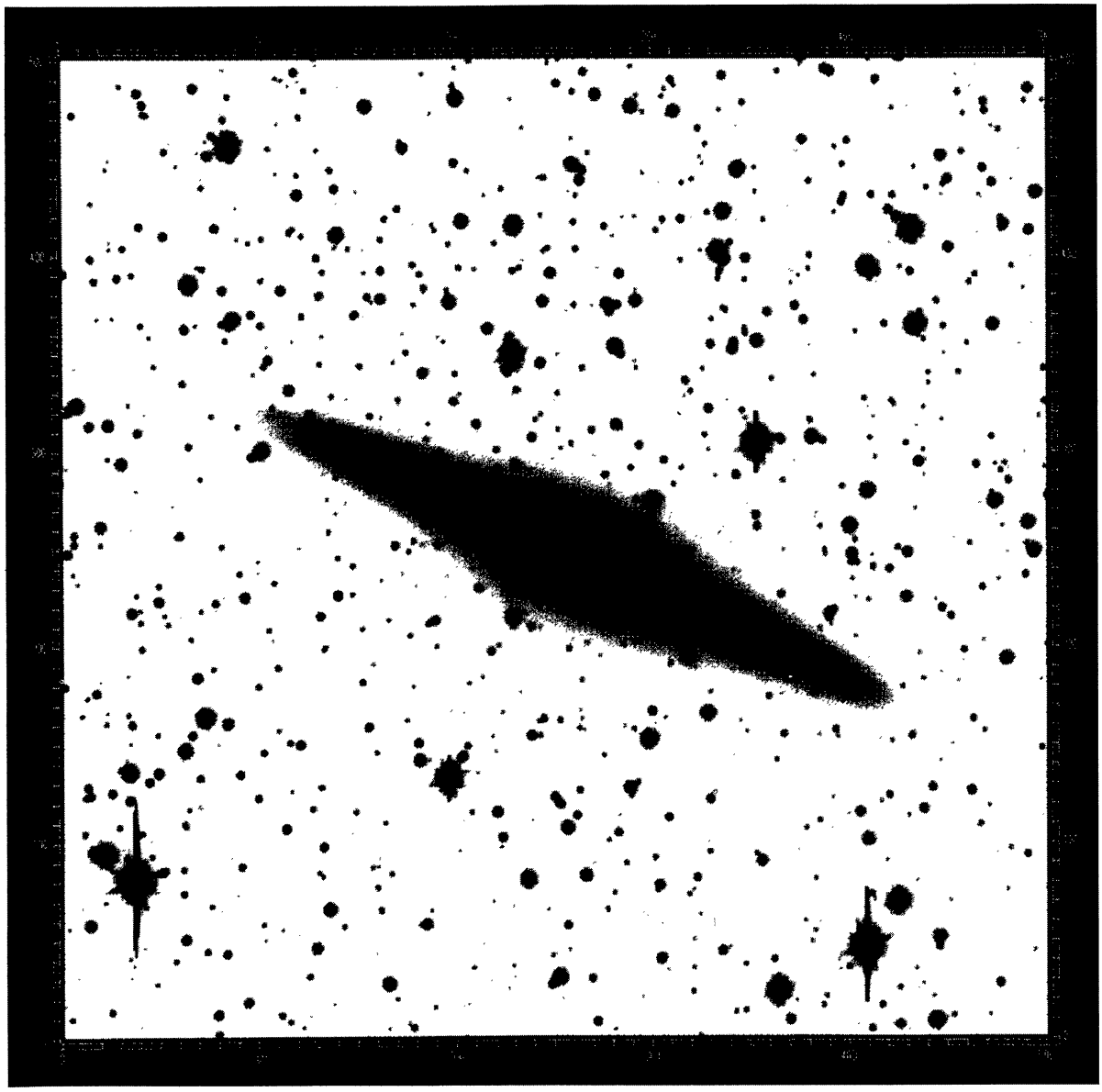

FIG. 1. Greyscale image of NGC 891, displayed using a log stretch to show the faint thick disk regions in the outer galaxy. North is to the right, East down. It can be seen that the thick disk isophotes are symmetrical (both with respect to different sides of the galaxy and above and below the plane), suggesting a dynamically well-mixed population.

Morrison *et al.* (see page 2062)

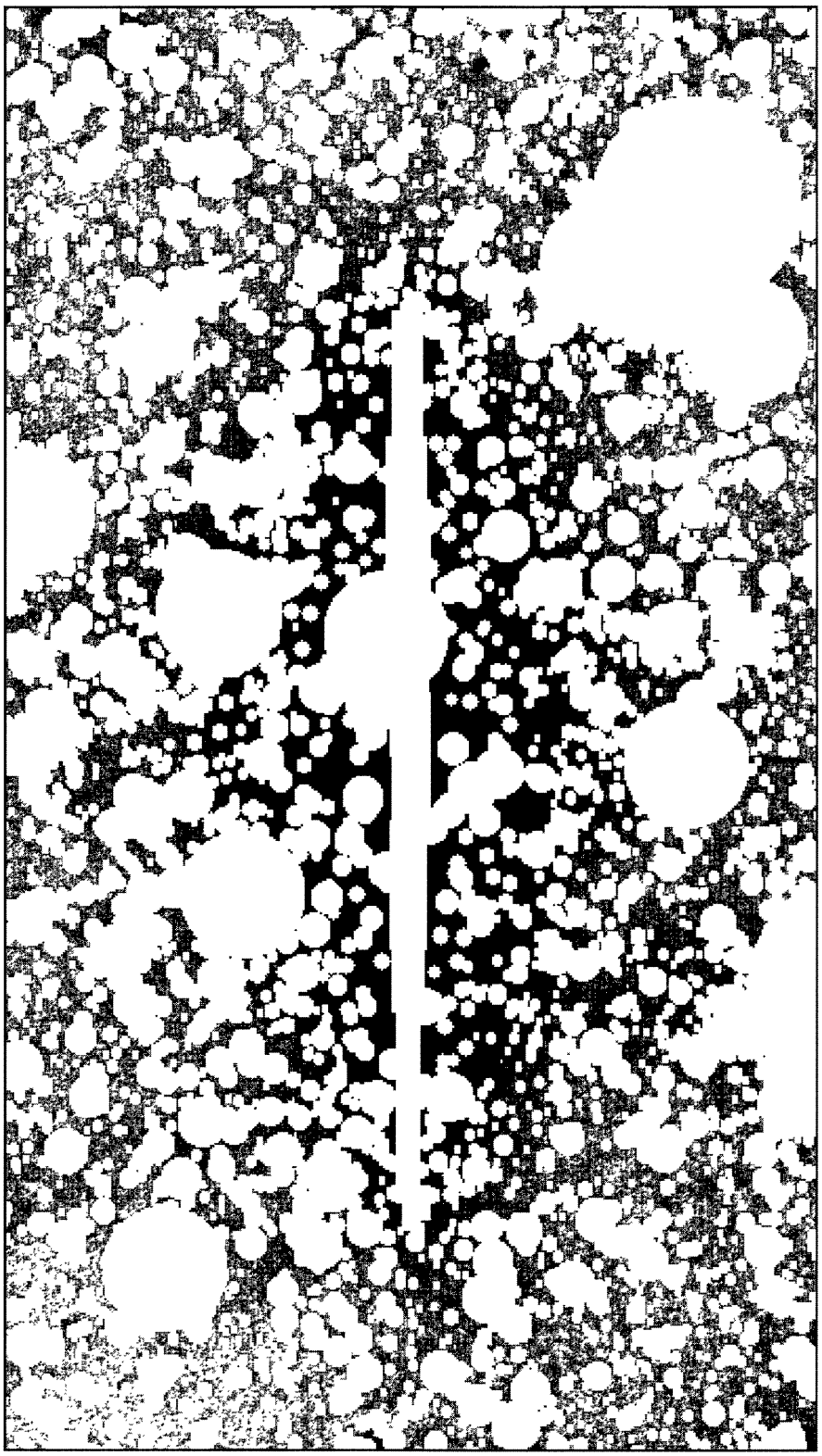

FIG. 4. The inner portion of the galaxy image with mask superimposed. The mask eliminates regions contaminated by dust, foreground stars, and other galaxies.

Morrison *et al.* (see page 2063)

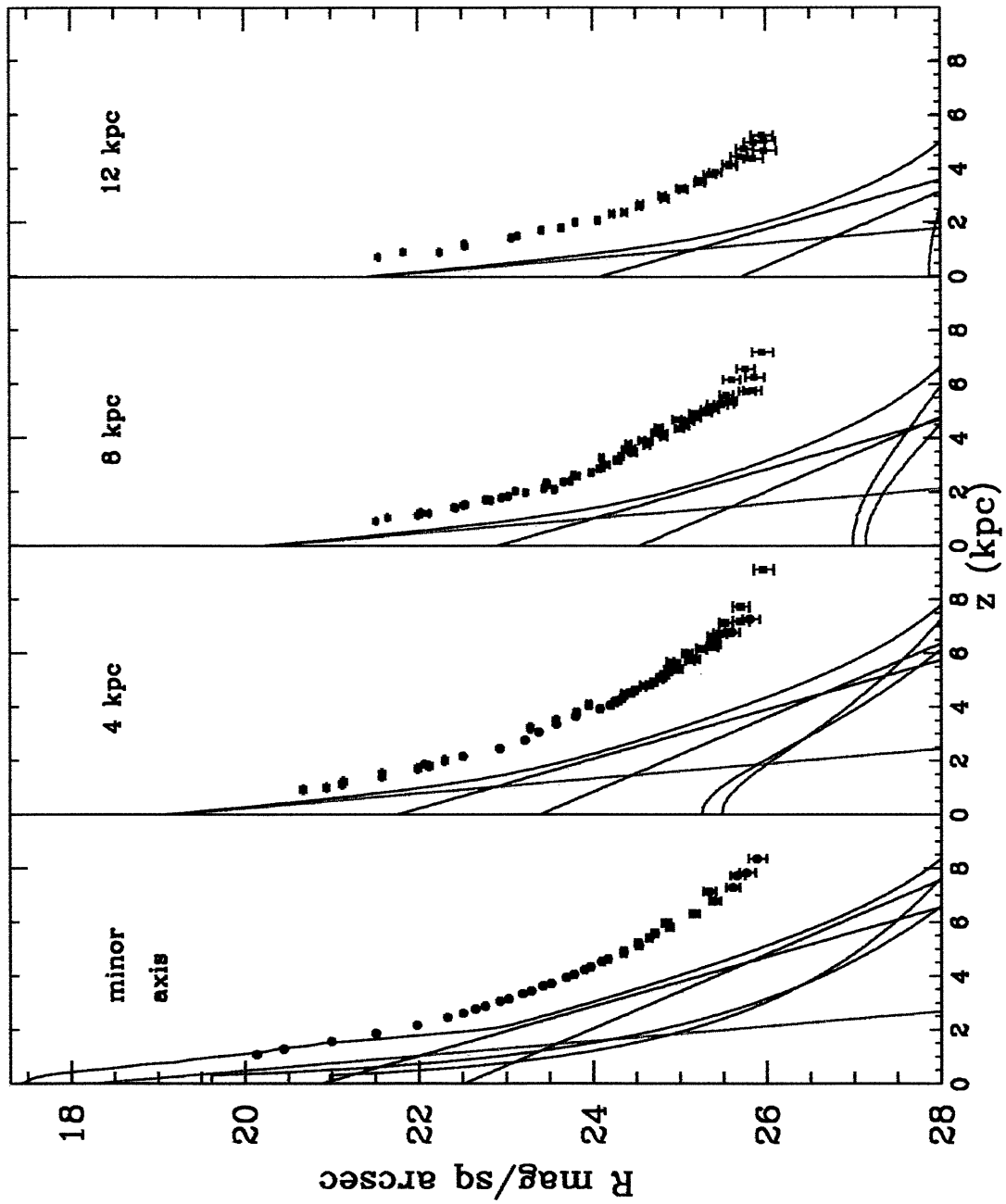

FIG. 8. This plot shows our model of the stellar populations of the Milky Way—red for thin disk, blue for thick disk and green for halo. The two lines for thick disk and halo show the range of current estimates of their properties. The solid black line shows total light, including the contribution of bulge/bar on the minor axis. For comparison, our photometry of NGC 891 is also shown. If the NGC 891 distance estimate is not seriously in error, NGC 891 is significantly more extended in the vertical direction than our Galaxy.